Colloids and Surfaces A: Physicochemical and Engineering Aspects 610 (2021) 125638

Contents lists available at ScienceDirect

Colloids and Surfaces A: Physicochemical and Engineering Aspects

journal homepage: www.elsevier.com/locate/colsurfa

Adsorption and corrosion inhibition characteristics of 2–(chloromethyl) benzimidazole for C1018 carbon steel in a typical sweet corrosion environment: Effect of chloride ion concentration and temperature

Moses M. Solomon [1,3,*], Ikenna B. Onyeachu [2], Demian I. Njoku [2], Simeon C. Nwanonenyi [2], Emeka E. Oguzie [2,*]

[1] Center of Research Excellence in Corrosion, King Fahd University of Petroleum & Minerals, Dhahran 31261, Saudi Arabia
[2] Africa Centre of Excellence in Future Energies and Electrochemical Systems (ACE-FUELS), Federal University of Technology, Owerri, Nigeria
[3] Department of Chemistry, College of Science and Technology, Covenant University, Canaanland, Km10, Idiroko Road, Ota, Ogun State, Nigeria

GRAPHICAL ABSTRACT

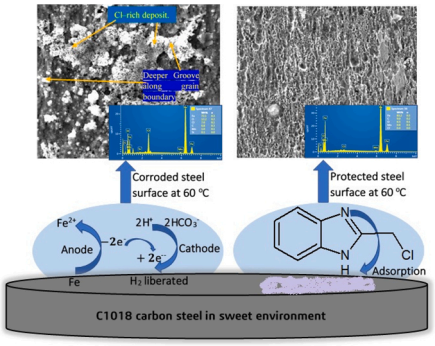

ARTICLE INFO

Keywords:
Sweet corrosion
Benzimidazole
Corrosion inhibition
Toxicity
Temperature
Carbon steel
.

ABSTRACT

Benzimidazole derivatives are emerging as promising corrosion inhibitors for oil and gas application because they exhibit high efficiency and very good environmental profile. Although long alkyl and phenyl chains enhance their efficiency, they also increase their toxicity. Finding benzimidazole derivatives devoid of long hydrocarbon chains and with lower toxicity has become a priority. 2–(chloromethyl)benzimidazole (CMB), with log $P_{o/w}$ = 2.2, has been investigated as a promising low-toxic sweet corrosion inhibitor for C1018 carbon steel in CO_2–saturated NaCl solution under static condition using experimental and theoretical approaches. At 25 °C, Open circuit potential (OCP), electrochemical impedance spectroscopy (EIS), and potentiodynamic polarization (PDP) techniques confirm that CMB is an anodic-type sweet corrosion inhibitor which is able to form a protective layer on the steel surface and provide inhibition efficiency of 97.54% at 10 ppm. The efficiency increased to 98.40% and 98.58% upon increasing the temperature to 40 °C and 60 °C, respectively but decreased to 96.32% and 94.76% as the salt concentration was raised to 5.0% and 7.0% NaCl, respectively. The latter was attributed to the antagonistic competition between Cl^- ions and CMB for anodic adsorption. The CMB–steel interaction is facilitated by the free electrons around N heteroatoms and C = C bonds, based on FTIR analysis and

* Correspondence:(Moses M. Solomon), (Emeka E. Oguzie).
E-mail addresses: moses.solomon@kfupm.edu.sa (M.M. Solomon), emeka.oguzie@futo.edu.ng (E.E. Oguzie).

https://doi.org/10.1016/j.colsurfa.2020.125638
Received 23 July 2020; Received in revised form 7 September 2020; Accepted 23 September 2020
Available online 15 October 2020

computational calculations. This eventually ameliorates the surface degradation of the steel during the sweet corrosion at 25 and 60 °C. CMB performance is highly comparable with reported sweet corrosion inhibitors with higher toxicity values.

1. Introduction

Sweet corrosion is the most significant corrosion challenge for steel–based crude oil transportation pipelines in the petroleum industry. It is a severely localized corrosion which is triggered by the aqueous phase of petroleum; composed of CO_2 gas dissolved in saline drilling solutions [1]. Its cost implications and resultant material damage are humongous. Currently, the petroleum industry encourages strict adherence to the standards of the Paris commission (PARCOM) regulation [2] when developing highly effective sweet corrosion inhibitors. One of the most important standards is the value of partition coefficient, log $P_{o/w}$, which describes the hydrophilicity or hydrophobicity of the inhibitor molecule. PARCOM has stipulated the standard log $P_{o/w} < 3$ for a non–toxic molecule. Higher log $P_{o/w}$ values indicate greater hydrophobicity, longer retention within the environment, and more toxicity [2].

The bulk of research into sweet corrosion inhibitors aims at discovering highly effective, more benign molecules which can replace the largely–used, but highly–toxic long–chain imidazolines [3–11]. The hydrocarbon chains enhance the adsorption and film formation by the imidazolines. However, they also impart detrimental toxicity; for example, increasing log $P_{o/w} = -0.8$ (for base imidazoline [12]) to log $P_{o/w} = 8.53$ (for oleyl imidazoline [13]). Recent research works have exposed imidazole and benzimidazole derivatives as highly effective sweet corrosion inhibitors and promising replacements for imidazolines [14–18]. Comparatively, these imidazoles and benzimidazoles exhibit far lower log $P_{o/w}$ values than the imidazolines. Nevertheless, close scrutiny reveals that their log $P_{o/w}$ values also depends on the nature of substituent attached to the parent molecule. For instance, the substitution of the NO_2 group (in 2-(4-nitrophenyl)-4,5-diphenyl-1H imidazole) with CH_3 (to yield 4,5-diphenyl-2-(p-tolyl) imidazole) increases log $P_{o/w}$ value from 4.9 to 5.4 [19,20]. Similarly, the log $P_{o/w}$ value of 2–phenylbenzimidazole changes significantly from 3.2 to 3.8 due to the attachment of a bromo group (to the phenyl substituent) and a methyl group (to the nitrogen atom in a benzimidazole ring) [21,22]. Consequently, identifying a benzimidazole derivative with lower log $P_{o/w}$ value than reported, so far, in the literature would be remarkable provided such benzimidazole delivers equally high efficiency against sweet corrosion.

2–(chloromethyl)benzimidazole (CMB), Fig. 1, is a benzimidazole derivative whereby a chloromethyl group is attached to the C–2 position of a benzimidazole moiety. Such attachment is significantly devoid of the usual phenyl groups and long alkyl chains reported in the literature. It confers Log $P_{o/w} = 2.2$ on CMB [23], which is appreciable lower than the values for other benzimidazole derivatives reported in the literature as sweet corrosion inhibitors. This makes CMB a novel low–toxic benzimidazole as sweet corrosion inhibitor. The low toxicity of CMB is further buttressed by its well–known anti–fungal and anti–bacterial properties [24,25]. From a corrosion perspective, CMB has been reported as highly efficient corrosion inhibitor for carbon steel in HCl solution [26] and Fe in 1 M HNO_3 [27]. To the best of our knowledge, CMB has not been reported as a sweet corrosion inhibitor. It is, therefore, important to investigate the inhibitive property of CMB against sweet corrosion of steel.

In the present work, therefore, electrochemical impedance spectroscopy (EIS) and potentiodynamic polarization (PDP) are harnessed as electrochemical techniques to analyze the kinetics and mechanism of CMB as sweet corrosion inhibitor for C1018 carbon steel in CO_2–saturated 3.5 % NaCl solution under static condition. The electrochemical techniques are complemented with scanning electron microscopy (SEM) and Fourier transform infrared (FTIR) spectroscopy for surface characterizations. Quantum chemical calculation and Monte Carlo simulation are employed for the purpose of providing molecular–level interpretation to the CMB inhibition mechanism. Given that salt concentration and temperature usually vary along a crude oil transportation pipeline, the present work also investigates the effect of NaCl concentration and temperature on the performance of CMB.

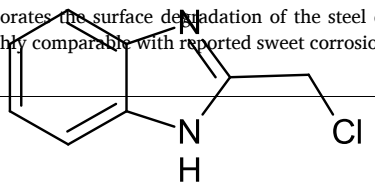

Fig. 1. Molecular structure of 2–(chloromethyl)benzimidazole (CMB).

2. Experimental

2.1. Preparation of electrodes and reagents

The C1018 carbon steel has elemental composition (wt. %) as: C (0.18), Mn (0.8), P (0.012), S (0.004), Si (0.028), Cu (0.14), Ni (0.04), Cr (0.05), Mo (0.01), Fe (balance). The steel sheets were cut into corrosion testing coupons with exposed surface area of 3.45 cm^2 after embedding in an epoxy resin. The sheets were cut into plane sheets with 1 cm^2 surface area for the surface characterization. The surfaces of the steel coupons were prepared by grinding, successively, with #400, #600 and #800 grit size silicon carbide papers. This was performed with simultaneous washing with distilled water, cleaning with acetone and drying with warm air. Analytical grade NaCl and 2–(chloromethyl)benzimidazole (CMB) were procured from Sigma Aldrich and used as supplied. The 3.5 % NaCl solution was prepared with distilled water, while CMB stock solution was prepared by dissolving 0.1 g of the inhibitor in 100 ml isopropanol.

2.2. Electrochemical corrosion testing

An assembly of the steel coupon as working electrode, a graphite rod as counter electrode and Ag/AgCl electrode as reference electrode, made up a three–electrode corrosion system. The corrosion testing was conducted with the aid of a Gamry Potentiostat (model 600) equipped with the Echem Analyst software for EIS curve fitting. The corrosion environment was a 500 mL corrosion cell containing 3.5 % NaCl solution saturated with CO_2 gas and yielding a pH of 3.8 ± 0.2. The CO_2 was, first, bubbled through the solution for 1 h before loading the coupon (and injecting the required CMB dose) and was continuously bubbled throughout the experiment. Inhibitor concentrations of 1.0, 5.0, 10.0, and 50.0 ppm were considered at 25 °C. Using an optimum CMB concentration, the effects of temperature (40 and 60 °C) and salt concentration (5.0 and 7.0 % NaCl) were also studied. During the electrochemical corrosion measurement, the working electrode was initially allowed to attain steady open circuit potential during 3600 s free corrosion in the test solution with and without CMB. At the open circuit potential, a sinusoidal excitation potential of ±10 mV was applied over the frequency range of 10^5 and 10^{-1} Hz to perform the EIS measurements. For the PDP measurements, the working electrode was polarized between +250 mV and −250 mV around the open circuit potential using a scan rate of 0.2 mVs^{-1}.

2.3. Surface characterization

For the surface characterization, the steel sample was freely immersed for 12 h in the CO_2–saturated 3.5 % NaCl solution without and with the optimum CMB concentration. The carefully scrapped corrosion

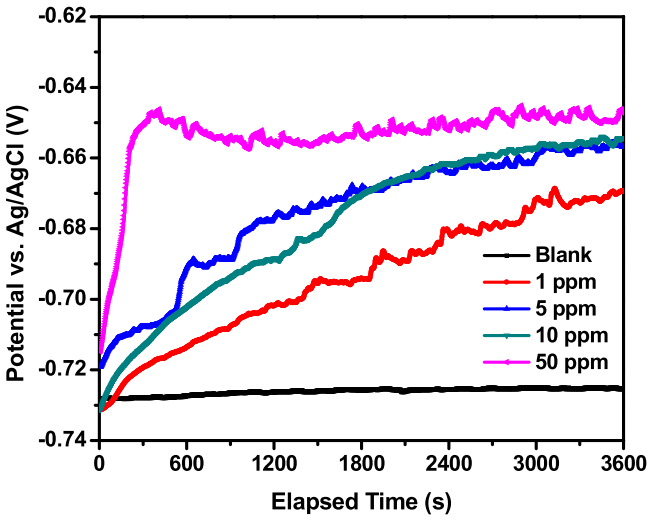

Fig. 2. Attainment of open circuit potential (OCP) during sweet corrosion of C1018 carbon steel in CO_2-saturated 3.5 wt% NaCl solution without and with different CMB concentrations at 25 °C.

layer formed on the steel surface, at 25 °C, was submitted for FTIR characterization using the attenuated total refection (ATR) mode in a Nicolet iS5 FTIR spectrophotometer equipped with an iD5 ATR. This characterization was necessary to ascertain the inhibitor action by adsorption mechanism. The surface morphology and elemental composition of the steel surface were acquired, after sweet corrosion at 25 and 60 °C, with a scanning electron microscope (SEM/EDAX Ziess Evo 50 XVP) hyphenated with an energy dispersive X-ray spectrophotometer (EDAX). This was necessary to investigate the effect of CMB on the localized corrosion of the carbon steel surface during the sweet corrosion.

2.4. Theoretical calculations

Density functional theory (DFT) software tool (Dmol3 and Forcite (Molecular dynamics tool) module respectively) of Material Studio 7.0 were employed to provide the chemical reactivity of CMB molecule and its interaction strength with Fe surface in the gas phase. Our previous works have shown that the Fe (110) is the most stable Fe phase in steel involved in the sweet corrosion [28]. The parameters used for the Dmol3 simulation include the followings; energy optimization task, functional correlation (LDA and PWC), Basis Set (DND), Basis file (3.5), Spin Unrestricted, Use symmetry, Multiplicity = 1, Charge = 0. The electronic parameters for molecular dynamics are; geometrical optimization task, COMPASS Energy, QEq Charge, super cell range 8 by 6, slap position of 1.00 Å, vaccum thickness of slab of 20 Å, Fe (110) crystal surface, quench dynamic task, quench every 250 steps, NVE Ensemble, time step of 1.0, total simulation time of 5.0 and average of five energy samples.

3. Results and discussion

3.1. Sweet corrosion inhibition by CMB at 25 °C

3.1.1. Open circuit potential (OCP)

The variation of OCP with time for C1018 sample in CO_2–saturated 3.5 % NaCl solution without and with CMB is shown in Fig. 2. A steady-state OCP around −730 mV is noticed throughout the acquisition period for the steel in the absence of CMB. The presence of CMB induces a shift of OCP towards anodic potential regions. The displacement resides between +60 and +90 mV, shifting more anodically with increase in CMB concentration. Consequently, CMB behaves as an anodic inhibitor based on previous definitions [28,29]. The OCP, as a thermodynamic property, indicates the metal susceptibility to dissolution in the corrosion medium. The positive shift of OCP in the presence of CMB signifies that the inhibitor adsorption decreases the tendency of the steel surface to corrode in the brine solution. The direct relationship between the CMB concentration and extent of OCP displacement can be attributed to increased thickening and greater protection by the adsorbed inhibitor film. This can be evidenced by the OCP behavior in the presence of 50 ppm CMB whereby a sharp potential displacement occurs during the initial 400 s which remains constant, thereafter, until 3600 s.

3.1.2. Electrochemical impedance spectroscopy (EIS)

Fig. 3 presents the EIS results obtained during the sweet corrosion of C1018 carbon steel in CO_2–saturated 3.5 % NaCl solution without and with different CMB doses at 25 °C. The Nyquist representations in Fig. 3a have the shapes of semicircles both in the absence and presence of CMB. The shapes indicate charge transfer–controlled corrosion phenomena [30–33]. Larger Nyquist semicircles are observed in the presence of CMB, which clearly indicate increased corrosion resistance. Also, a degradation phenomenon of impedance is observed in the CMB inhibited Nyquist semicircles relative to the uninhibited loop and is associated with the delay in the charge transfer process due to the building up of the CMB film on the carbon steel surface [34,35]. The plots presented in Fig. 3b and 3c describe the Bode phase angle and absolute impedance formats of the EIS results, respectively. Single phase angle peak with maximum around 60° is noticed for the steel in the absence of CMB. The corresponding value of absolute impedance is around 2 Ωcm^2. The single-phase angle peak is consistent with the charge transfer–controlled corrosion phenomena described by the equivalent circuit in Fig. 4a. It is a single time constant that models the sweet corrosion using a solution resistance (R_s), a constant phase element (CPE_{dl}) and a charge transfer resistance (R_{ct}). The R_s describes the resistance between the steel surface and the tip of the Luggin capillary holding the reference electrode. The CPE_{dl} describes the charge capacitance at the steel–solution interface which, in turn, influences the rate of electron transfer and, hence, rate of corrosion. The R_{ct} indicates the resistance to charge transfer across the interface and is a measure of corrosion resistance. Usually, the choice of CPE over a pure capacitor, in an equivalence circuit model, is to account for the effect of surface inhomogeneity of the corroding steel surface on the charge capacitance at the interface [36,37]. The Eq. (1) describes how the impedance of a CPE (Z_Q) can be deduced; whereby Y_o is the modulus of admittance, j is an imaginary unit ($j^2 = -1$), w is the angular frequency, and α ($-1 \leq \alpha \leq 1$) is the CPE exponent. The values of the relevant EIS parameters are provided in Table 1.

$$Z_Q = Y_0^{-1}(jw)^{-\alpha} \quad (1)$$

The addition of CMB to the CO_2-saturated brine solution increases the size of Nyquist semicircles (Fig. 3a), the phase angle peaks (Fig. 3b) and the values of absolute impedance (Fig. 3c). The phase angle transforms from a single peak (at 1 and 5 ppm) into two peaks (at 10 and 50 ppm). This single peak–to–two peaks transition shows that CMB molecules go from merely occupying the electric double layer (at lower concentration) to becoming a well–developed film on the steel surface (at higher concentration). The adsorbed film becomes more protective with increase in CMB concentration, as observed by the higher phase angle peaks in the presence of 50 ppm CMB compared with 10 ppm. The inhibitor adsorption creates two interfaces on the steel surface: a film–solution interface (high frequency phase angle peak) and a steel–solution interface beneath the inhibitor film (low frequency phase angle peak). Consequently, the equivalent circuit model in Fig. 4b was adopted to describe the sweet corrosion of the carbon steel in CO_2–saturated 3.5 % NaCl solution at 25 °C in the presence of CMB. The property of the inhibitor film–solution interface is defined by the film pore resistance (R_f) and the charge capacitance at the interface (CPE_f). On the other hand, the CPE_{dl} and R_{ct} define the properties of the steel–solution interface beneath the adsorbed inhibitor film. The values of

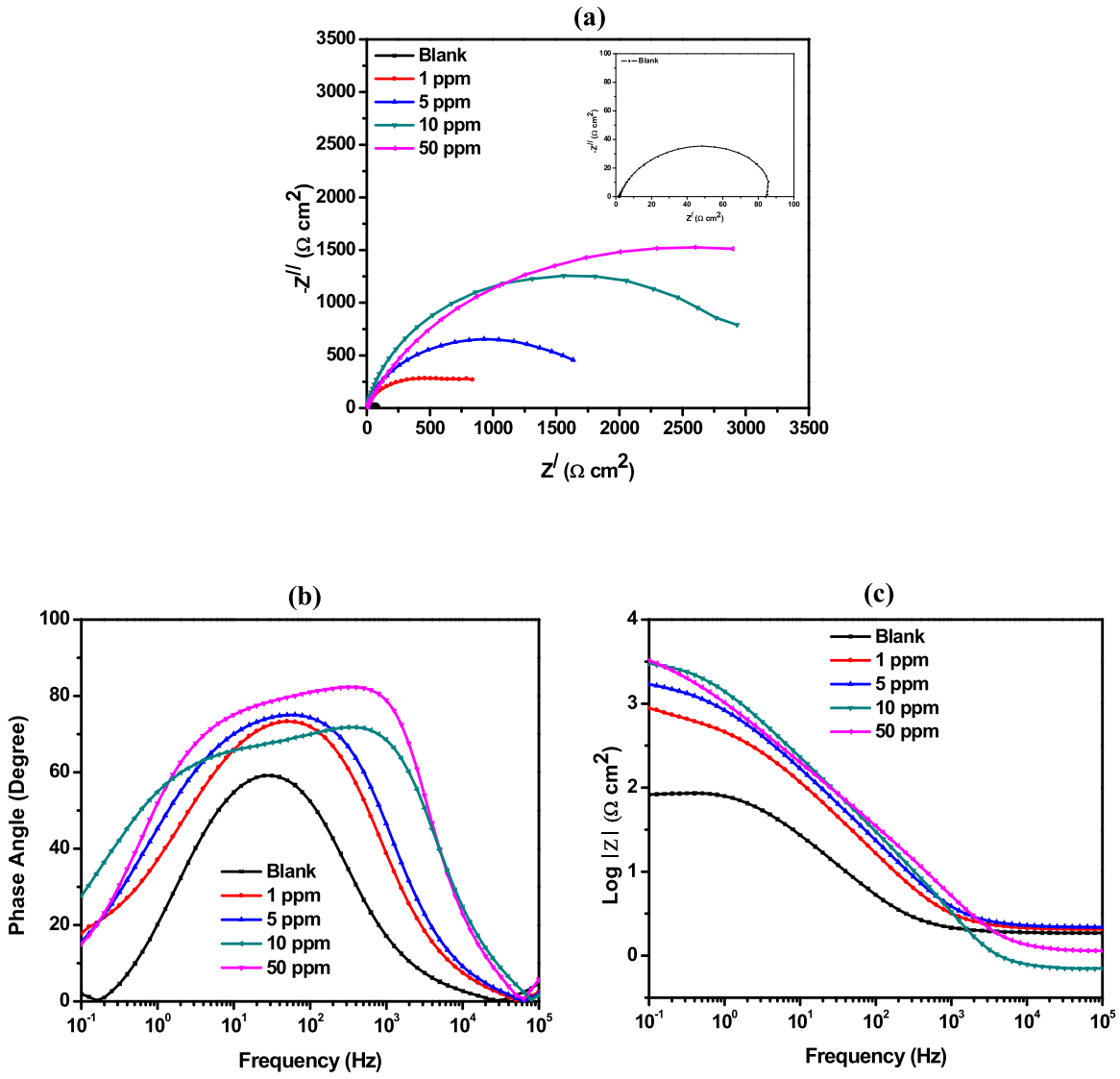

Fig. 3. EIS spectra obtained during sweet corrosion of C1018 carbon steel in CO_2-saturated 3.5 wt% NaCl solution without and with different CMB concentrations at 25 °C, expressed in (a) Nyquist (b) Phase angle and (c) absolute impedance formats.

the EIS parameters are detailed in Table 1.

Based on Table 1, the steel sample yields R_{ct} value of 85 ± 2.96 Ω cm^2 in the absence of CMB. The R_{ct} value becomes 1036 ± 2.12 Ω cm^2 and 3411 ± 4.14 Ω cm^2 when 1 ppm and 50 ppm CMB are, respectively, added. Nevertheless, the inhibitor film provides additional resistance (R_f) that augments the R_{ct} so as to yield a total resistance, R_t, of 1091 ± 8.49 Ω cm^2 (with 1 ppm) and 3920 ± 5.66 Ω cm^2 (with 50 ppm). Accordingly, CMB provides a maximum inhibition efficiency (% η) of 97.83 ± 0.10 % at 50 ppm, based on Eq. (2). In the equation, the total resistance obtained without and with CMB is, respectively, signified by $R_{t(blank)}$ and $R_{t(inh)}$. The increase in R values occurs with decrease in Y values. This is because, during adsorption, corrosion inhibitor molecules would displace H_2O molecules and other aqueous species that propagate corrosion on the steel surface. Thus, the quantity of charge admitted into the double layer (Y_{dl}) decreases in the presence of CMB which, eventually, decreases the rate of charge transfer across the double layer (R_{ct}).

$$\%\eta_{EIS} = 1 - \frac{R_{t(blank)}}{R_{t(inh)}} \times 100\% \quad (2)$$

3.1.3. Potentiodynamic polarization (PDP)

The PDP plots in Fig. 5 depict the response of the C1018 carbon steel during polarization in CO_2–saturated 3.5 % NaCl solution without and with different CMB concentrations at 25 °C. Based on the Eq. (3)–(6), H^+ ion reduction and Fe oxidation are, respectively, the most dominant cathodic and anodic half–processes controlling the sweet corrosion of the C1018 carbon steel [38]. The oxidation of Fe furnishes the electrons which sustain the H^+ reduction. By extrapolating the PDP curves around ±10 mV of cathodic–anodic transition potential, the relevant polarization parameters such as corrosion current density (i_{corr}), corrosion potential (E_{corr}) and the Tafel constants (β_a and β_c) were deduced. The i_{corr} is usually a measure of the corrosion rate, whereas the E_{corr} values describe how plausible it is for the steel to undergo sweet corrosion [30]. The values of these polarization parameters are detailed in Table 2.

The addition of increasing CMB doses persistently shifts the E_{corr} value more anodically from −730 mV (without CMB) to −621 mV (with 50 ppm CMB). This is consistent with the observation from the OCP measurement and confirms that CMB lowers the susceptibility for the steel to dissolve in the solution by behaving like an anodic inhibitor. This anodic mechanism is also seen in Fig. 5 whereby the CMB addition causes more significant reduction in the anodic arm of the PDP plots. Thus, CMB molecules inhibit the sweet corrosion by adsorbing on the anodic sites of the steel surface where they suppress the rate of Fe → Fe^{2+} transformation. The inhibitor can achieve this by furnishing free

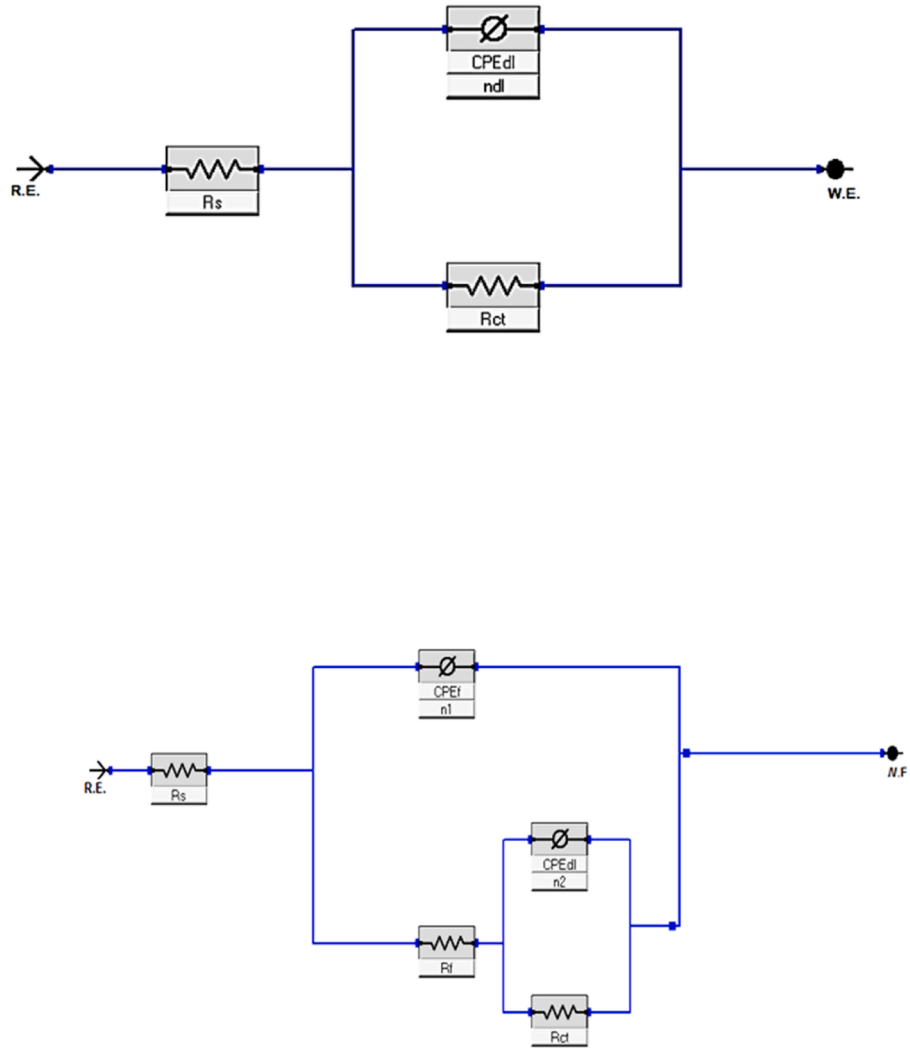

Fig. 4. Equivalent circuit model proposed for C1018 carbon steel during sweet corrosion in CO_2-saturated 3.5 wt% NaCl solution (a) without and (b) with CMB at 25 °C.

Table 1
EIS parameters obtained during sweet corrosion of C1018 carbon steel in CO_2–saturated 3.5 % NaCl solution without and with different CMB concentrations at 25 °C.

Conc. (ppm)	R_s (Ω cm^2)	CPE_d		R_{ct} (Ω cm^2)	CPE_f		R_f (Ω cm^2)	($R_{p\ =\ } R_f + R_{ct}$) (Ω cm^2)	Goodness of Fit ($\times 10^{-3}$)	% η
		Y_{dl} (μFcm^{-2} s^{n-1})	α_{dl}		Y_f (μFcm^{-2}sn^{-1})	α_f				
0	1.88 ± 0.001	1047 ± 21.21	0.84 ± 0.000	85 ± 2.96	-	-	-	85 ± 2.96	1.52 ± 0.004	–
1	2.09 ± 0.006	897 ± 3.54	0.44 ± 0.001	1036 ± 2.12	177 ± 3.54	0.91 ± 0.001	55 ± 3.56	1091 ± 8.49	0.41 ± 0.028	92.21 ± 0.31
5	2.21 ± 0.000	182 ± 0.42	0.45 ± 0.000	2204 ± 5.66	109 ± 2.12	0.92 ± 0.001	83 ± 0.14	2287 ± 8.49	0.18 ± 0.110	96.29 ± 0.16
10	1.97 ± 0.001	152 ± 0.14	0.47 ± 0.000	2862 ± 3.54	94 ± 0.14	0.93 ± 0.000	496 ± 2.12	3358 ± 8.49	1.01 ± 0.010	97.54 ± 0.01
50	2.13 ± 0.006	141 ± 4.24	0.67 ± 0.001	3411 ± 4.14	74 ± 4.24	0.93 ± 0.001	509 ± 0.42	3920 ± 5.66	0.66 ± 0.010	97.83 ± 0.10

electrons (localized around the nitrogen moieties and pi–bonds within the aromatic ring) to interact with the unoccupied d–orbitals of the Fe atoms. It is also possible that CMB could exist as a protonated species like many other benzimidazoles in acidic media [14,17]. In this way, CMB interacts electrostatically with negatively–charged Cl– ion primarily adsorbed on the steel surface due to Fe^{2+} generation. Anyways, by decreasing the rate of Fe → Fe^{2+} transformation, the adsorbed CMB molecules shunt electron transfer intended to sustain the H^+ reduction process at the cathodic sites. As a result, the i_{corr} value is significantly reduced from 73.10 μA cm^{-2} (without CMB) to 3.50 μA cm^{-2} (with 50 ppm CMB). From the PDP results, the inhibition efficiency of CMB ($\%\ \eta_{PDP}$) was calculated based on Eq. (7), where $i_{corr(blank)}$ and $i_{corr(inh)}$ indicate, respectively, the corrosion current density in the absence and presence of CMB. The values follow the same trend as calculated from the EIS results, such that inhibition efficiency increases with CMB concentration attaining a maximum of 95.21 % with 50 ppm.

Table 2
Polarization parameters obtained during sweet corrosion of C1018 carbon steel in CO_2–saturated 3.5 % NaCl solution without and with different CMB concentrations at 25 °C.

Conc. (ppm)	E_{corr} (mV/Ag/AgCl)	i_{corr} (μA cm^{-2})	β_a (mV dec^{-1})	$-\beta_c$ (mV dec^{-1})	% η_{PDP}
0	–730	73.10	26	195	–
1	–669	6.06	53	171	91.71
5	–655	4.89	58	174	93.31
10	–645	3.81	62	171	94.79
50	–621	3.50	70	189	95.21

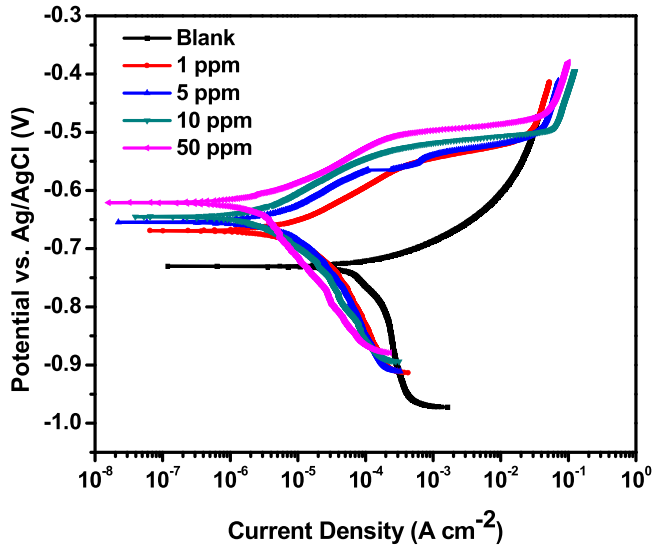

Fig. 5. PDP plots obtained during sweet corrosion of C1018 carbon steel in CO_2-saturated 3.5 wt% NaCl solution without and with different CMB concentrations at 25 °C.

$$2H^+_{(aq)} + 2e^- \rightarrow H_{2(g)}; (pH < 4) \quad (3)$$

$$2H_2CO_{3(aq)} + 2e^- \rightarrow H_{2(g)} + 2HCO^-_{3(aq)} \quad (4); (pH\ 4-6)$$

$$2HCO^-_{3(aq)} + 2e^- \rightarrow H_{2(g)} + 2CO^{2-}_{3(aq)}; (pH \geq 6) \quad (5)$$

$$Fe_{(s)} \rightarrow Fe^{2+}_{(aq)} + 2e^- \quad (6)$$

$$\%\eta_{PDP} = 1 - \frac{i_{corr(inh)}}{i_{corr(blank)}} \times 100\% \quad (7)$$

3.2. Effect of sweet corrosion variables

The electrochemical measurements have shown that CMB is a highly efficient inhibitor against the sweet corrosion of C1018 carbon steel at 25 °C. However, the results also show that the inhibition efficiency of CMB did not appreciate significantly beyond 10 ppm. In the present work, therefore, the effects of salt concentration (5.0 and 7.0 wt.% NaCl) at 25 °C, and temperature (40 and 60 °C) were considered without and with 10 ppm CMB.

3.2.1. Effect of NaCl concentration

The results acquired from the EIS and PDP measurements during the sweet corrosion of the C1018 carbon steel in 3.5 %, 5.0 % and 7.0 % NaCl are provided in Fig. 6. In the Nyquist results, Fig. 6(a), the semicircle size continuously increase in size as the NaCl concentration increases. Similar trend is observed in the Bode Phase angle peaks and the values of absolute impedance. The EIS results still show a single time constant for the steel corrosion in the absence of CMB. The equivalent circuit model in Fig. 4(a) is, therefore, still relevant to interpret the influence of salt concentration on the sweet corrosion mechanism of C1018 carbon steel without the inhibitor. The persistent increase in sizes of Nyquist semicircles and Phase angle peaks suggest that the corrosion resistance of the C1018 steel increases with the NaCl concentration. This finding is consistent with previous reports [39–41]. Zeng et al. [42] reported that the solubility of CO_2 in NaCl solution decreased from 0.032 M to 0.023 M as the salt concentration increased from 0.1 wt.% to 10 wt.%. This implies continuous decrease in the concentration of resultant H_2CO_3 (hence, concentration of H^+ and HCO^-_3 ions) in the sweet corrosion environment. Consequently, the quantity of charge percolation and rate of transfer across the steel–solution interface are sure to be minimized. This is the reason that, based on Table 3, the admittance (Y_{dl}) continuously decrease while the R_{ct} increases as NaCl concentration increases.

From the PDP plots in Fig. 6(d), the change of NaCl concentration shifts E_{corr} more cathodically and has insignificant effect on the anodic phenomenon (Fe oxidation). Instead, the change in salt concentration influences the cathodic reactions. Slightly, but consistently, the cathodic current shifts to lower value with more NaCl in solution. The insignificant effect on anodic reactions and consistent decrease in cathodic current are also in agreement with the model proposed by Han et al. [41]. The findings confirm that the effect of increasing NaCl concentration, during sweet corrosion of steel, is to lower the rate of reduction reactions with respect to H^+ and HCO^-_3 concentration. After extrapolation, Table 4 shows that the corrosion current density shifts from 73.10 μA cm^{-2} (in 3.5 % NaCl) to 35.00 μA cm^{-2} (in 7.0 % NaCl).

In the presence of CMB, the increase in NaCl concentration is observed to cause a shrinkage in the size of Nyquist semicircles (Fig. 7 (a)). This indicates that the inhibition properties of CMB is diminished by the higher NaCl concentration. In the corresponding Bode plots, the weakening of one of the two impedance peaks could be observed in Fig. 7(b), while the value of absolute impedance, Fig. 7(c), consistently decreases with increase in NaCl concentration. The observation in Fig. 7 (b) can be related to the deteriorating integrity of the adsorbed inhibitor film on the steel surface. The increase in NaCl concentration from 3.5 % to 5.0 % obscures the high frequency phase angle peak while the low frequency peak remains prominent. This could indicate a thinning of the adsorbed CMB film. Further increase in NaCl concentration to 7.0 % suppresses the low frequency phase angle peak while the high frequency peak remains dominant. This is attributed to a degraded steel–solution interface beneath the adsorbed CMB film. Summarily, increasing NaCl concentration from 3.5 % to 5.0 % and then to 7.0 % decreases the thickness of the adsorbed film and encourages the ingress of corrosion–causing species into the electric double layer. Therefore, the adsorption integrity between CMB film and the steel surface becomes weakened. While increasing the NaCl concentration enhances the resistance of C1018 steel during sweet corrosion in the absence of an inhibitor, it appears that the increasing Cl^- ion concentration in the solution antagonizes the performance of CMB. Since increased NaCl concentration decreases the concentration of H^+ and HCO^-_3 ions but increases Cl^- ion concentration, it must be the higher Cl^- ion concentration in the electric double layer that intensifies the attack on the steel surface rather than promote the electrostatic attraction that leads to CMB adsorption. Hence, the R_{ct} values decrease persistently in the presence of CMB while the reverse is noticed for the Y_{dl}. Eventually, the efficiency of inhibition by CMB declines from 97.54 ± 0.01 % (with 3.5 % NaCl) to 94.76 ± 0.14 (with 7.0 % NaCl), as seen in Table 3.

The effect of the increasing Cl^- ion concentration is further shown by the PDP plots in Fig. 7(d). Although both anodic and cathodic current densities are shifted to higher values as NaCl concentration increases, the increase in anodic current is more salient than the cathodic current. Given that increasing NaCl concentration diminishes the concentration of H^+ and HCO^-_3 ions, it is expected that the fixed CMB concentration (10 ppm) should effectively decrease the cathodic current as NaCl

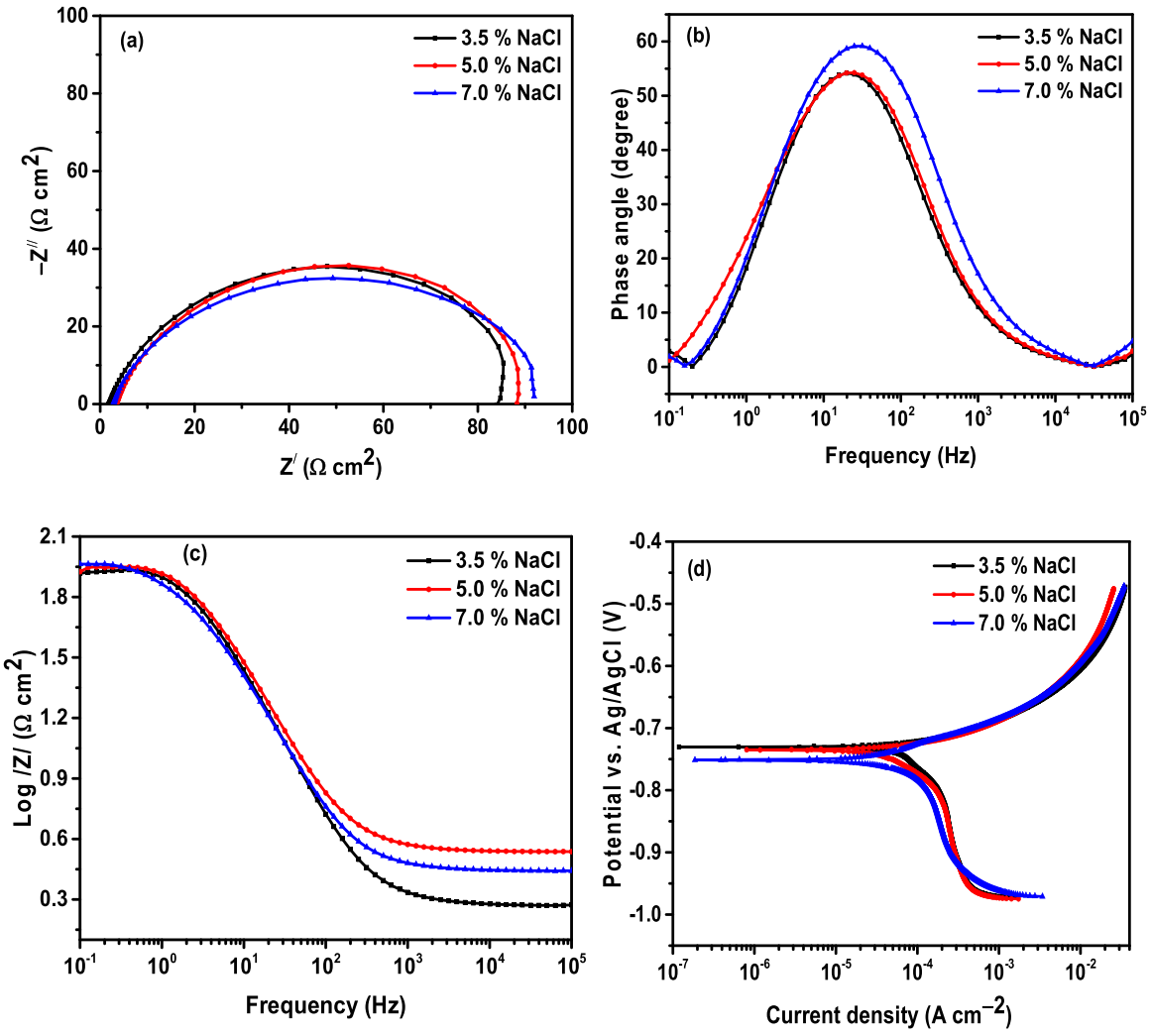

Fig. 6. Plots showing (a) Nyquist (b) Phase angle (c) absolute impedance and (d) PDP results obtained during sweet corrosion of C1018 carbon steel in CO_2-saturated 3.5, 5.0 and 7.0 % NaCl solution without CMB at 25 °C.

Table 3
EIS parameters obtained during sweet corrosion of C1018 carbon steel in CO_2–saturated 3.5, 5.0 and 7.0% NaCl solution without and with 10 ppm CMB concentration at 25 °C.

Conc. (ppm)	R_s (Ω cm^2)	CPE_{dl}		R_{ct} (Ω cm^2)	CPE_f		R_f (Ω cm^2)	($R_p = R_f + R_{ct}$) (Ω cm^2)	Goodness of Fit ($\times 10^{-3}$)	% η
		Y_{dl} (μFcm^{-2} s^{n-1})	α_{dl}		Y_f (μFcm^{-2}sn^{-1})	α_f				
					3.5 % NaCl					
0	1.88 ± 0.001	1047 ± 21.21	0.84 ± 0.000	85 ± 2.96	-	-	-	85 ± 2.96	1.52 ± 0.004	–
10	1.97 ± 0.001	152 ± 0.14	0.47 ± 0.000	2862 ± 3.54	94 ± 0.14	0.93 ± 0.000	496 ± 2.12	3358 ± 8.49	1.01 ± 0.010	97.54 ± 0.01
					5 % NaCl					
0	2.46 ± 0.001	959 ± 7.07	0.84 ± 0.003	87 ± 1.41	-	-	-	88 ± 1.41	1.71 ± 0.031	–
10	2.21 ± 0.000	230 ± 9.19	0.42 ± 0.001	2325 ± 2.96	111 ± 1.41	0.93 ± 0.000	62 ± 0.14	2387 ± 4.24	0.57 ± 0.003	96.32 ± 0.05
					7 % NaCl					
0	2.15 ± 0.011	935 ± 6.36	0.80 ± 0.006	90 ± 1.96	-	-	-	95 ± 1.96	0.48 ± 0.055	–
10	1.97 ± 0.001	403 ± 0.14	0.32 ± 0.000	1775 ± 2.12	260 ± 2.12	0.89 ± 0.001	36 ± 0.14	1811 ± 2.83	0.77 ± 0.028	94.76 ± 0.14

Table 4
Polarization parameters obtained during sweet corrosion of C1018 carbon steel in CO_2–saturated 3.5, 5.0 and 7.0% NaCl solution without and with 10 ppm CMB concentration at 25 °C.

Conc. (ppm)	E_{corr} (mV/Ag/AgCl)	i_{corr} (μA cm^{-2})	β_a (mV dec^{-1})	$-\beta_c$ (mV dec^{-1})	% η_{PDP}
3.5 % NaCl					
0	–730	73.10	26	195	–
10	–645	3.81	62	171	94.79
5 % NaCl					
0	–735	38.60	20	93	–
10	–658	4.48	61	146	88.39
7 % NaCl					
0	–751	35.00	20	50	–
10	–659	5.50	64	147	84.29

concentration increases. The contrary observation, however, shows that CMB is less of a cathodic inhibitor. On the other hand, the more significant increase in anodic current implies that Cl^- ion concentration has more influence on CMB adsorption than H^+ and HCO_3^- ions. The more the Cl^- ion in the solution, the more shielded are the CMB molecules from adsorbing on the anodic sites. This is very consistent with the EIS result which showed that increasing Cl^- ion weakens the CMB–steel interface and could promote the delamination of the CMB film from the steel surface. Consequently, Fe oxidation and steel dissolution is facilitated. The effects cumulatively increase the i_{corr} values, as Table 4 reveals. Regardless of this, however, the addition of 10 ppm CMB to the sweet corrosion environment with different NaCl concentrations at 25 °C improves the corrosion resistance of the C1018 steel to the tune of 84.29 % inhibition efficiency in 7.0 % NaCl solution.

3.2.2. *Effect of temperature*

The effect of temperature on the sweet corrosion behavior of C1018 carbon steel in CO_2–saturated 3.5 % NaCl solution is elucidated in the EIS and PDP plots in Fig. 8. As the temperature is elevated from 25 °C to 60 °C, the EIS Nyquist semicircles (Fig. 8(a)) continuously shrink in size, the phase angle peaks are lowered (Fig. 8(b)) and the values of absolute impedance also decrease (Fig. 8(c)). These trends imply that the temperature rise increases the rate of sweet corrosion. This is rational given that, at higher temperature, corrosion agents acquire greater kinetic energy that enables them migrate faster towards the electric double layer where they increase the rate of charge transfer across the double layer. The values of EIS parameters acquired, based on the equivalence model in Fig. 4, are detailed in Table 5. The temperature rise from 25 °C to 60 °C, respectively, decreases the R_{ct} value from 85 ± 2.96 Ω cm^2 to

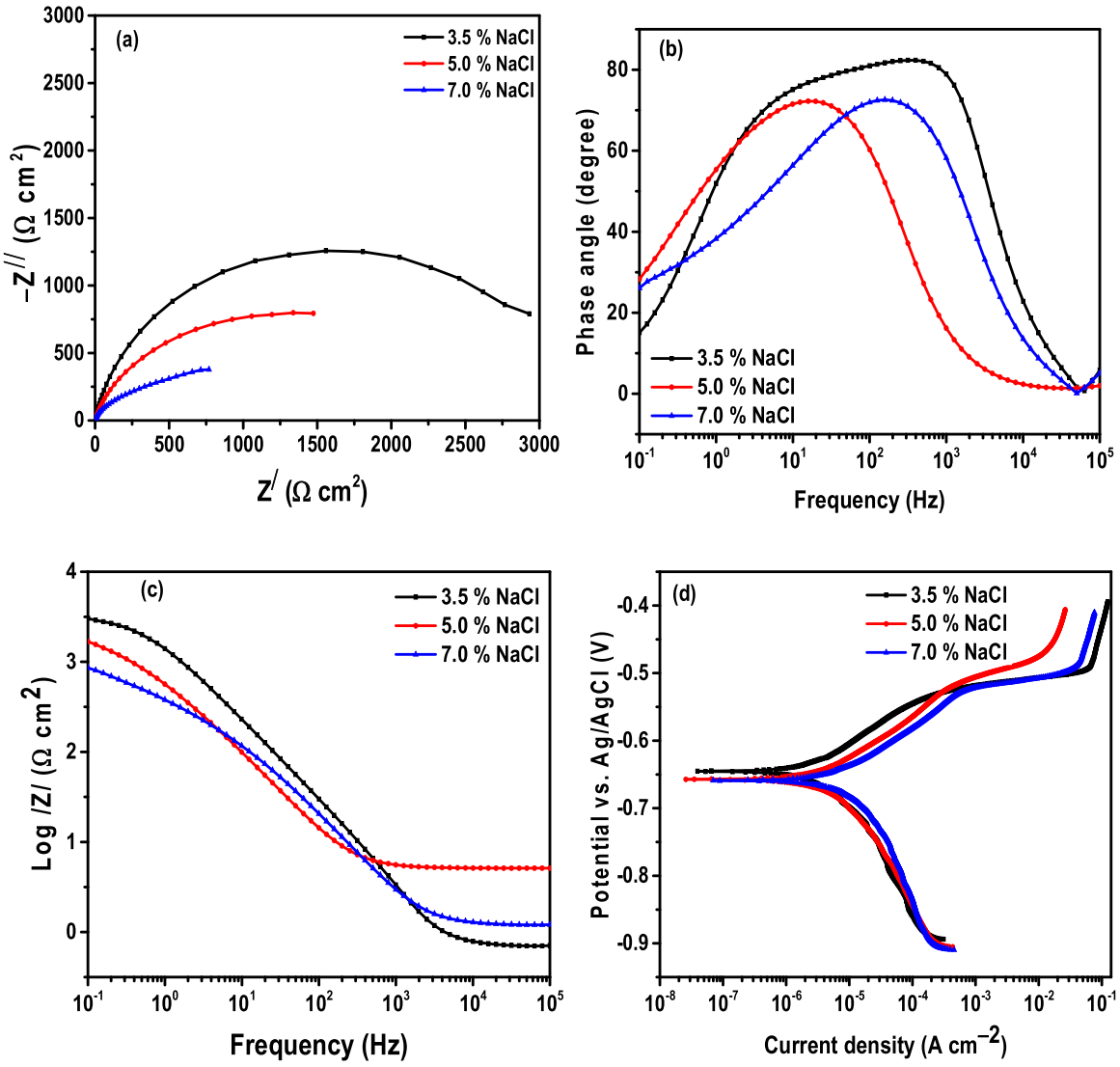

Fig. 7. Plots showing (a) Nyquist (b) Phase angle (c) absolute impedance and (d) PDP results obtained during sweet corrosion of C1018 carbon steel in CMB–containing CO_2–saturated 3.5, 5.0 and 7.0 % NaCl solution without CMB at 25 °C.

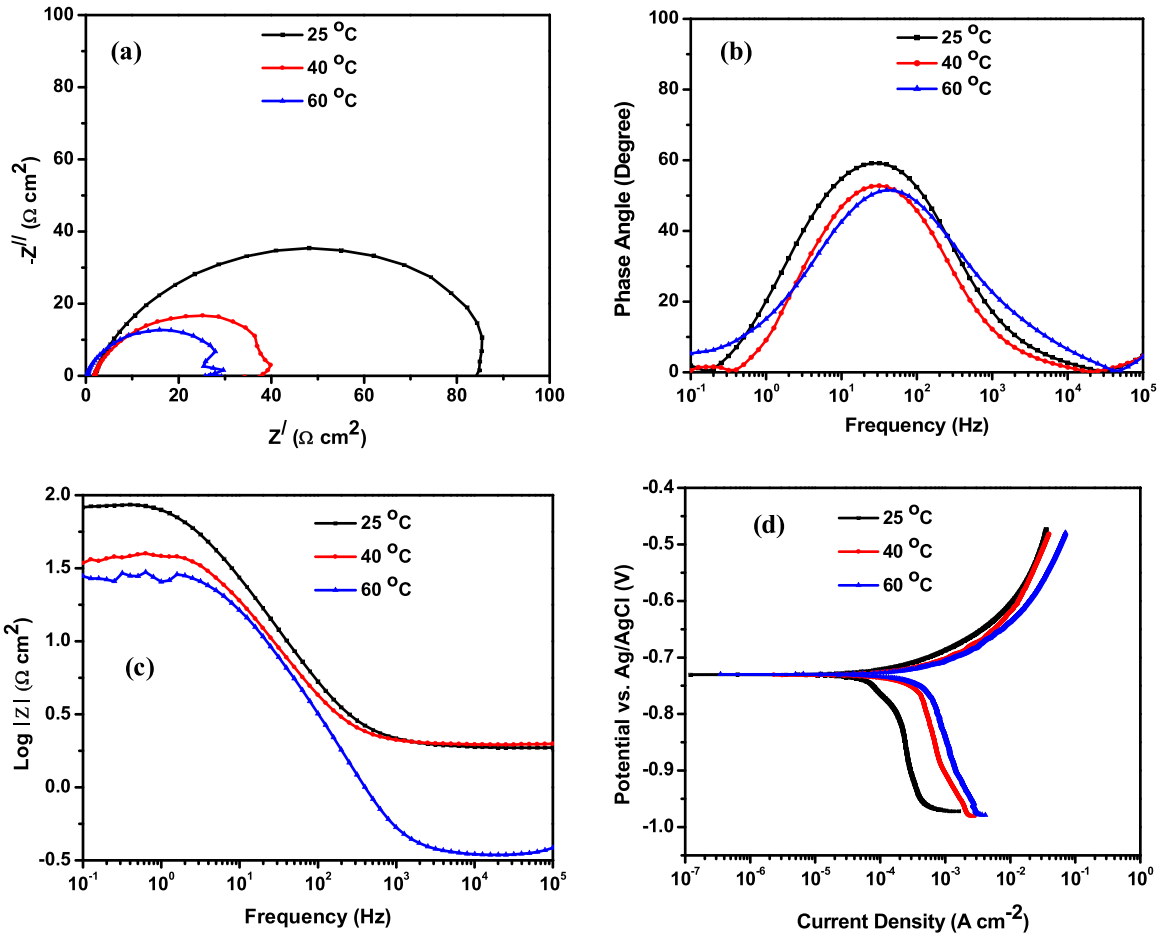

Fig. 8. Plots showing (a) Nyquist (b) Phase angle (c) absolute impedance and (d) PDP results obtained during sweet corrosion of C1018 carbon steel in CO_2–saturated 3.5 % NaCl solution without CMB at 25, 40 and 60 °C.

Table 5
EIS parameters obtained during sweet corrosion of C1018 carbon steel in CO_2–saturated 3.5% NaCl solution without and with 10 ppm CMB concentrations at 25, 40 and 60 °C.

Conc. (ppm)	R_s (Ω cm^2)	CPE_{dl}		R_{ct} (Ω cm^2)	CPE_f		R_f (Ω cm^2)	($R_p = R_f + R_{ct}$) (Ω cm^2)	Goodness of Fit ($\times 10^{-3}$)	% η
		Y_{dl} (μFcm^{-2} s^{n-1})	α_{dl}		Y_f (μFcm^{-2}sn^{-1})	α_f				
					25 °C					
0	2.46 ± 0.001	1047 ± 21.21	0.84 ± 0.000	85 ± 2.96	-	-	-	85 ± 2.96	1.52 ± 0.004	–
10	1.97 ± 0.001	152 ± 0.14	0.47 ± 0.000	2862 ± 3.54	94 ± 0.14	0.93 ± 0.000	496 ± 2.12	3358 ± 8.49	1.01 ± 0.010	97.54 ± 0.01
					40 oC					
0	1.90 ± 0.018	1210 ± 6.36	0.76 ± 0.000	38 ± 0.71	-	-	-	38 ± 0.71	2.85 ± 0.028	–
10	2.44 ± 0.001	831 ± 2	0.43 ± 0.010	1955 ± 2.14	130 ± 3.41	0.88 ± 0.001	417 ± 5.02	2372 ± 9.90	0.56 ± 0.010	98.40 ± 0.01
					60 oC					
0	2.33 ± 0.009	1265 ± 3.54	0.76 ± 0.000	28 ± 0.16	-	-	-	28 ± 0.16	1.21 ± 0.072	–
10	2.32 ± 0.002	899 ± 9.19	0.41 ± 0.007	1660 ± 4.24	102 ± 1.41	0.93 ± 0.000	307 ± 0.00	1967 ± 5.66	0.26 ± 0.003	98.58 ± 0.01

28 ± 0.16 Ω cm^2. The Y_{dl} also increases while the n values decrease as an indication of the increased roughness of the steel surface due to the corrosion.

In the PDP plots, Fig. 8(d), it could be seen that the elevation of sweet corrosion temperature from 25 °C to 60 °C does not alter the position of E_{corr}. Rather, a clear increase in both anodic and cathodic current densities is observed. This is due to the accumulation of corrosion–causing species at the steel–solution interface. Therefore, the rate of reduction of H^+ and HCO_3^- ions, and the rate of oxidation attack by Cl^-ions, are increased. It is well–known that, during sweet corrosion, higher temperature favors the precipitation of $FeCO_3$ and plausible formation of the well–developed protective scale during sweet corrosion

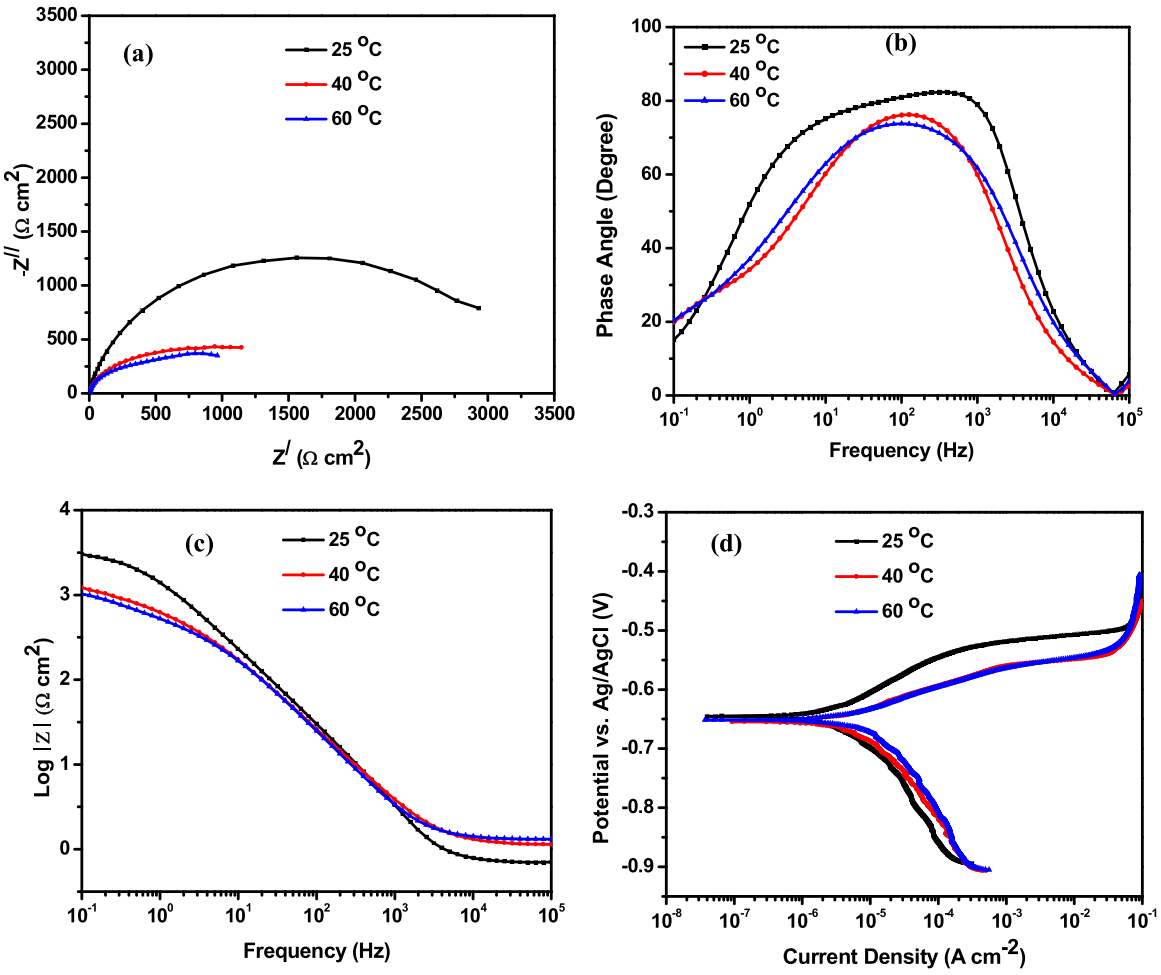

Fig. 9. Plots showing (a) Nyquist (b) Phase angle (c) absolute impedance and (d) PDP results obtained during sweet corrosion of C1018 carbon steel in CMB–containing CO_2–saturated 3.5 % NaCl solution without CMB at 25, 40 and 60 °C.

[42–45]. Nevertheless, no passivation phenomenon is observed in the PDP plots of Fig. 8(d). This implies that no well–developed $FeCO_3$ scale is formed at temperature up to 60 °C. This result is, therefore, consistent with other reports in the literature which acknowledge that the formation of well–developed $FeCO_3$ scale only occurs at temperature equal to (or greater than) 90 °C [45].

In the presence of 10 ppm CMB, increasing the temperature of the sweet corrosion environment also leads to decrease in the Nyquist semicircle sizes, phase angle maxima and absolute impedance values, as depicted in Fig. 9(a–c), respectively. It shows that the performance of CMB is limited by the temperature of the sweet corrosion environment. According to Table 5, an increase in temperature from 25 °C to 60 °C lowers the R_{ct} value from 2862 Ω cm^2 to 1660 Ω cm^2. It is affirmation that higher temperature increases the energy of corrosion agents and promotes their saturation of the double layer at the steel surface. Although the rise in temperature should also energize and promote migration of CMB molecules towards the steel surface, the higher concentration of H^+, HCO_3^- and Cl^- ions blocks the adsorption of CMB and increase both cathodic reduction of H^+ and HCO_3^- ions, and the anodic attack by Cl^- ions. It is also plausible that the elevated temperature increases the quantity of CMB desorbed from the steel surface, thereby, exposing more active sites for corrosion. This trend showcases the CMB adsorption mechanism as physiosorption rather than chemisorption. Accordingly, the CMB film on the steel surface becomes more incoherent and more porous, as confirmed by the continuous shift of R_f towards lower value in Table 5. Howbeit, the inhibition efficiency of CMB increases slightly with the rise in temperature and a maximum efficiency of 98.58 ± 0.01 % could be obtained at 60 °C.

Table 6
PDP parameters obtained during sweet corrosion of C1018 carbon steel in CO_2–saturated 3.5% NaCl solution without and with 10 ppm CMB concentrations at 25, 40 and 60 °C.

Conc. (ppm)	E_{corr} (mV/Ag/AgCl)	i_{corr} (μA cm^{-2})	β_a (mV dec^{-1})	$-\beta_c$ (mV dec^{-1})	% η_{PDP}
25 °C					
0	–730	73.10	26	195	–
10	–645	3.81	62	171	94.79
40 °C					
0	–731	206.00	37	183	–
10	–651	4.40	65	141	97.86
60 °C					
0	–730	230.0	29	173	–
10	–654	6.56	68	148	97.15

Similar with the observation in the blank solution, the increase in temperature also has insignificant effect on the E_{corr} value in the presence of CMB. The cathodic and anodic currents are also shifted to higher values, supporting the increased activity of H^+, HCO_3^- and Cl^- ions. Nevertheless, the change in anodic arm is more pronounced than observed with the cathodic arm. This suggests that, in the inhibited solution, CMB adsorbed film is more negatively impacted by Cl^- ions (at anodic sites) than by H^+ and HCO_3^- ions. This is true because the increased activity of H^+, due to temperature rise, does not result in a commensurate increase in cathodic current, as Fig. 9(d) reveals. Rather,

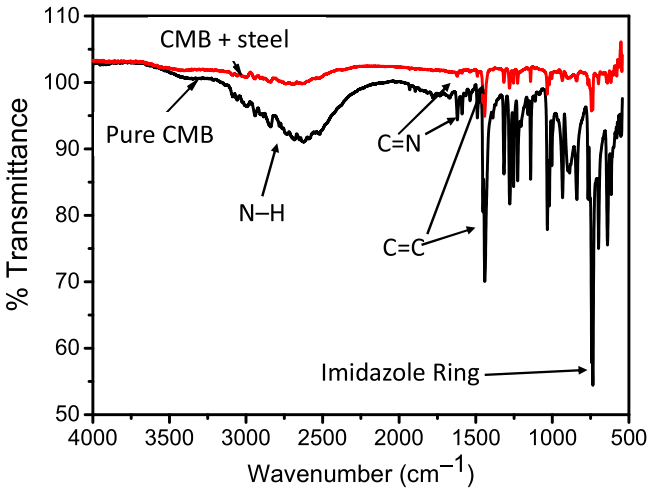

Fig. 10. FTIR spectra acquired for pure CMB and the surface of CMB–inhibited C1018 steel after sweet corrosion in CO_2–saturated 3.5 % NaCl solution without CMB at 25 °C.

it is the enhancement of Cl^- ion activity that causes a significant increase in anodic current. Moreover, the behavior of CMB at elevated temperature shows that the inhibitor adsorption is more of a physical process than chemical. Overall, Table 6 shows that the change in temperature from 25 °C to 60 °C increases the i_{corr} value from 3.81 μA cm^{-2} to 6.56 μA cm^{-2}. Nevertheless, the inhibition efficiency increases to the tune of 97.15 % at 60 °C, in agreement with the trend observed in the EIS result.

3.3. Surface characterization

3.3.1. FTIR characterization

The FTIR spectra obtained for the pure CMB and for the corrosion layer on the C1018 carbon steel after sweet corrosion in the presence of CMB are presented in Fig. 10. The pure CMB show strong and broad adsorption peaks spanning from 3200 cm^{-1}–2500 cm^{-1}. These signals are attributed to the N–H stretching functionality which was reported to exhibit strong intermolecular hydrogen bonding in the solid state [46]. The peak around 1675 cm^{-1} is due to the C = N functional group while the imidazole ring bending peak is seen around 750 cm^{-1} [47]. The peak due to C = C bonds in the aromatic ring are observed around 1500 cm^{-1}. Several absorption peaks could be found between 1350 and 1150 cm^{-1} which are attributed to C–H vibrations [46]. On the steel surface after sweet corrosion in the presence of CMB, some of the most important peaks in the CMB molecule can be seen. Such peaks include those due to N–H, C–N, C = C, and even the imidazole ring. The detection of these peaks confirms the adsorption of CMB as a mechanism for inhibiting the sweet corrosion of the C1018 carbon steel. The spectra reveal that the CMB molecules interact with the steel surface using the aforementioned functional groups (N–H, C–N, C = C). These groups contain free electrons that are donated to the Fe atoms on the steel surface. The finding is consistent with the mechanism of sweet corrosion inhibition by other benzimidazole derivatives [14,42].

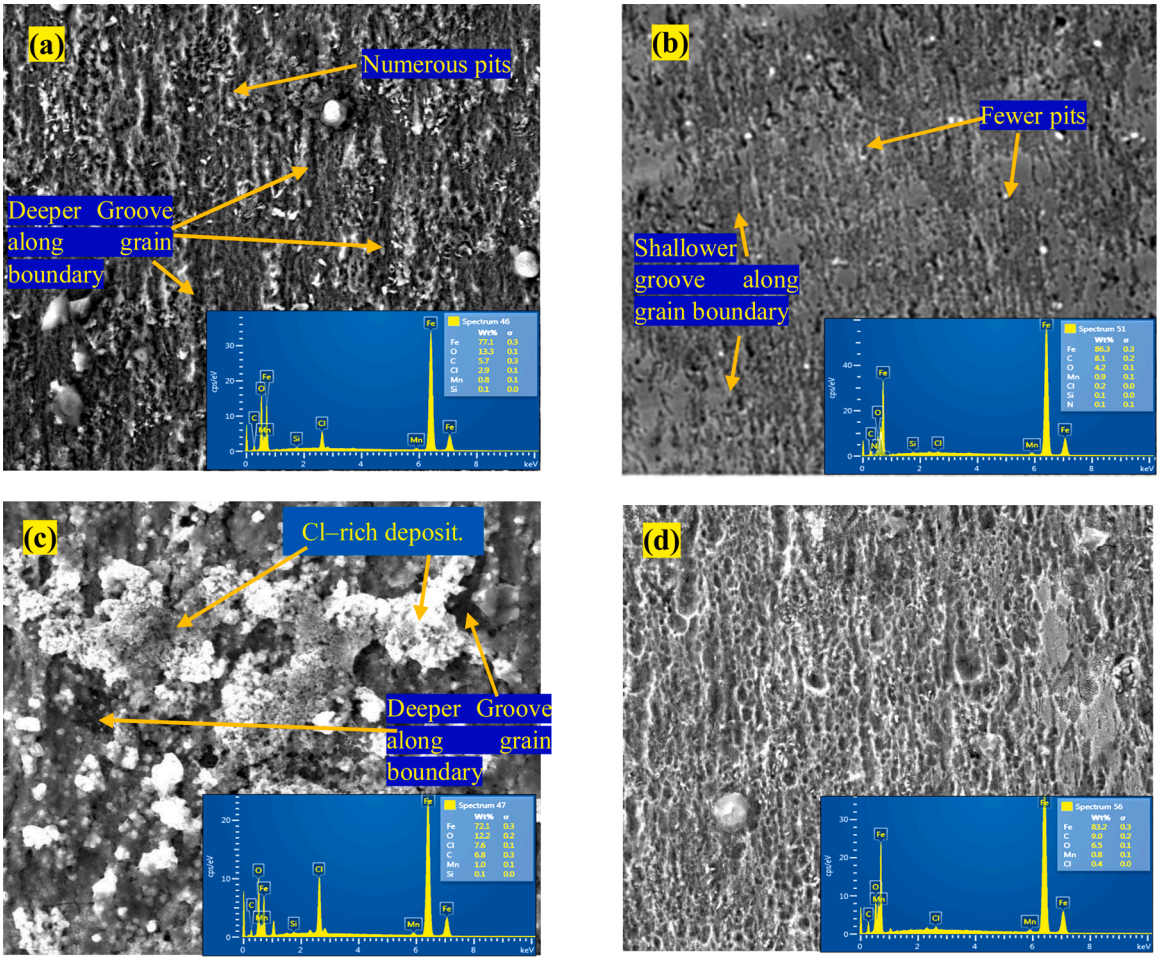

Fig. 11. SEM surface morphology with EDAX elemental composition acquired for C1018 carbon steel after sweet corrosion in CO_2-saturated 3.5 wt% NaCl solution (a) without and (b) with 10 ppm CMB at 25 °C and (c) without and (d) with 10 ppm CMB at 60 °C.

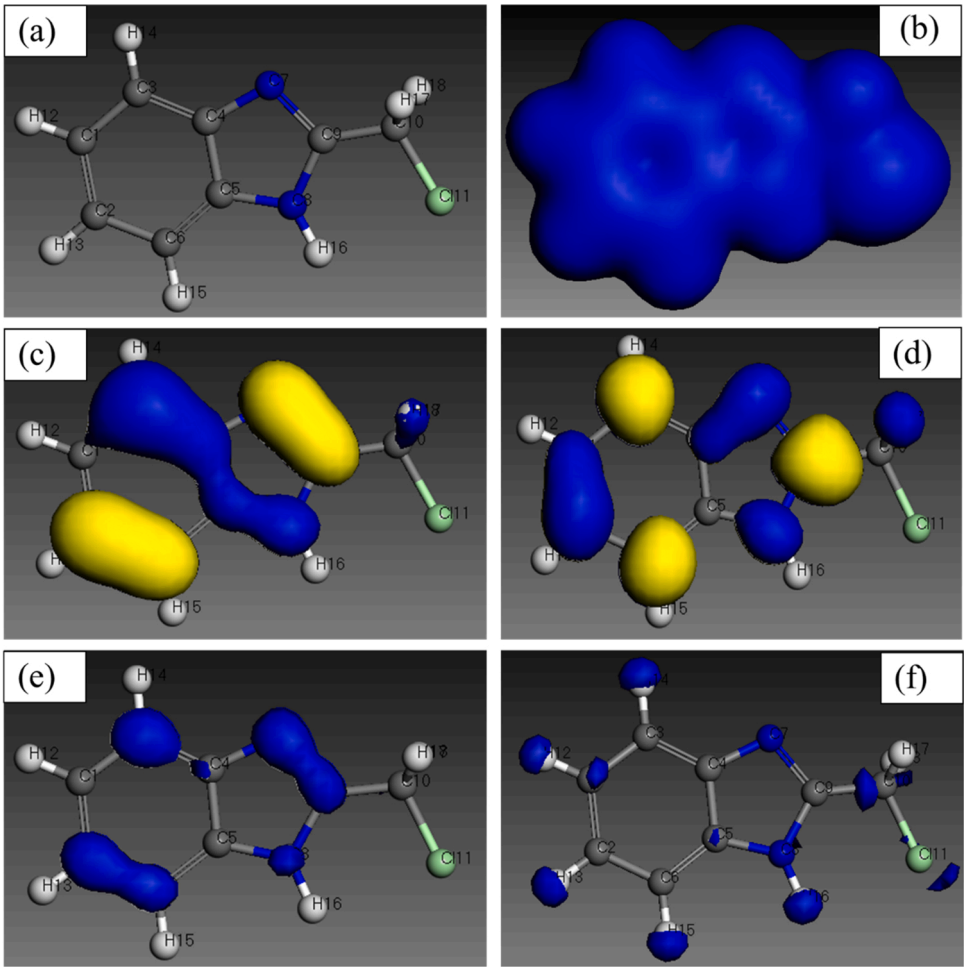

Fig. 12. (a) Optimized molecular structure, (b) frontiers orbitals distribution, (c) HOMO, (d) LUMO, (e) electrophilic attack (F−) and (f) nucleophilic attack (F+) of CMB.

3.3.2. SEM characterization

The SEM micrographs in Fig. 11(a–d) show the surface morphology of the C1018 carbon steel after sweet corrosion in 3.5 % NaCl solution without and with 10 ppm CMB at 25 and 60 °C. In the absence of CMB at 25 °C, Fig. 11(a), the steel surface exhibits severe roughness due to localized corrosion attack. Such localized corrosion is a well–known feature of sweet corrosion. Numerous pits inundate the steel surface and groove–like features form along the grain boundaries. Such localized surface degradation could, especially, be attributed to the attack by Cl^- ions. The addition of CMB to the sweet corrosion environment at 25 °C significantly minimizes this localized corrosion attack. The pits and groves become fewer and shallower. This is attestation that the adsorbed CMB film isolates the steel surface from corrosion agents. The protection ability of the CMB film can also be seen from the EDAX elemental analysis inserted in each SEM image. Comparing Fig. 11(a) with 11(b), a higher percentage of Fe and Cl in the absence of CMB could imply greater loss of Fe atoms from the steel surface due to Cl attack.

As temperature of the sweet corrosion environment increases to 60 °C in the absence of CMB, Fig. 11(c) shows more severe corrosion attack compared to the phenomenon at 25 °C shown in Fig. 11(a). The grooves become deeper and a significant portion of the steel surface is covered with crystalline deposits enriched with Cl. Thus, the rise in temperature favors greater Cl attack that promotes the steel dissolution. The increase in steel dissolution indicates greater loss of Fe atoms from the steel surface. This could explain why there is a decrease in the elemental composition of Fe and increase in the composition of Cl due to the temperature increase in the absence of CMB (compare Fig. 11(a) with 11 (c)). Compared with the observation in the blank solution, the steel in CMB–inhibited CO_2–saturated 3.5 % NaCl solution presents less deteriorated surface morphology after sweet corrosion at 60 °C (Fig. 11(d)). However, this morphology is more corroded than the observation at 25 °C in the presence of CMB. The elemental composition of Fe is, again, greater in the presence of CMB than in the blank solution at this elevated temperature. This is strong indication that the CMB adsorption protects the Fe atoms from being lost due to dissolution during the sweet corrosion. The CMB adsorption reduces the activity of Cl^- ions, most probably, by adsorbing on anodic sites on the steel surface.

3.4. Theoretical consideration

In recent times, quantum chemical computations are often employed to complement experimental results in inhibition studies. It helps to predict the nature of interaction between an organic specie and metal surface. To this end, the efficacy of an inhibitor compound can be predicted on the basis of its susceptibility to undergo donor-acceptor interaction with a substrate [48,49]. Hence, to provide the frontal orbital properties of CMB so as to afford insights on its interaction tendencies, quantum chemical computation was performed using Density Functional Theory (DFT). The computed DFT parameters for CMB compound are illustrated in Fig. 12 including: the optimized molecular structure (a), electron density (b), the highest occupied frontier molecular orbital (HOMO, (c)), the lowest unoccupied frontier molecular orbital (LUMO, (d)), the sites for electrophilic attack (F−, (c)), and the sites for nucleophilic attack (F+, (f)) for CMB compound. The

Table 7
Result of the Monte Carlo simulation for the lowest adsorption configurations of CMB, on Fe (110).

Compound	E_{HOMO} (eV)	E_{LUMO} (eV)	μE (eV)	B.E (kcal/mol)
CMB	−5.3624	−2.3564	3.006	−116.8

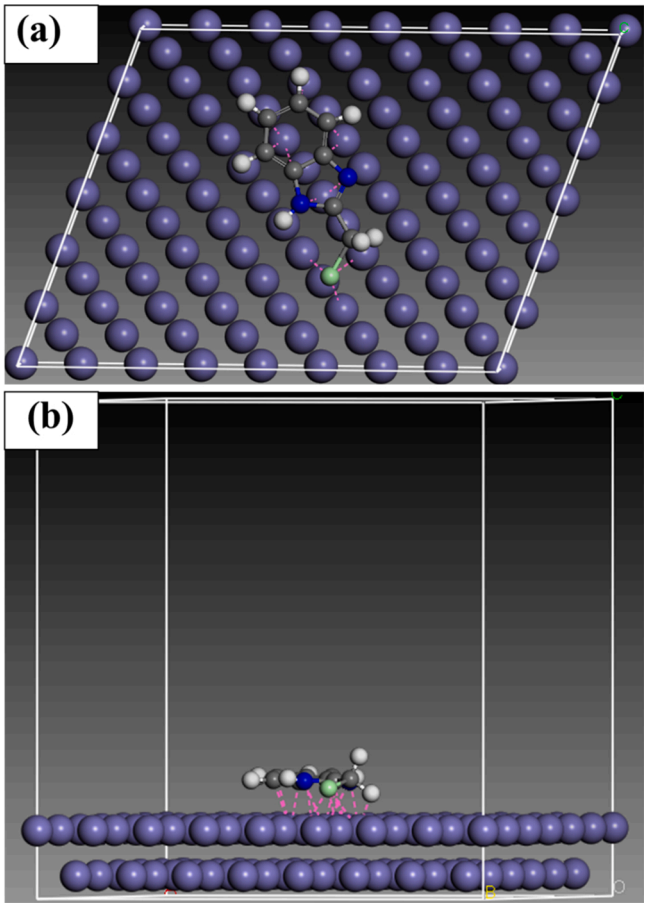

Fig. 13. (a) Top and (b) side views of the lowest adsorption orientation of CMB on the Fe (1 1 0) surface.

corresponding energies are listed in Table 7. Previous reports have shown that there is a correlation between the reactive behavior of a chemical compound and the distributions of HOMO and LUMO [48–50]. The HOMO frontier molecular electron distribution represents the electron donation sites, and LUMO represents the electron lacking sites of the inhibitor compound [48–50]. Likewise, (F−) is the site where electrophiles attack, while (F+) is the site where nucleophiles attack [51]. Inspection of the results presented in Fig. 12(b) reveal even distribution of electron–rich sites (for electrophilic attack or electron donation to vacant d-orbital of Fe) and electron–deficient sites (for nucleophilic attack or acceptance of electron from the dissolution of Fe using the anti-bonding orbitals) on CMB [52]. Based on Fig. 12(c,d), the HOMO and LUMO electrons are localized around the C = C and N groups in CMB. These are the points where electron donation and acceptance occur between CMB and the Fe atoms on the steel surface. These results are consistent with the results from FTIR characterization. The energy gap ($\mu E = E_{LUMO} - E_{HOMO}$) presented in Table 7 is an important index that reflects the tendency of a compound to undergo molecule–metal interaction. The lower the value of ΔE, the softer and easily polarizable (more reactive) the compound and vice versa [53]. Hence, the lower value of ΔE for CMB (Table 7) which is comparable/lower than other previously reported effective inhibitive additives [53–55] reflects the high

Table 8
: Comparing the inhibition efficiency of CMB with some reported sweet corrosion inhibitors with well–known log $P_{o/w}$ values.

Corrosion Inhibitor	Conc.	Sweet corrosion condition	% IE	Ref.
CMB (log $P_{o/w}$ = 2.2)	10 ppm	3.5 % NaCl + Static @ 25 °C 3.5 % NaCl + Static @ 60 °C	95 98	This work
N-Ethyl-2-undecyl-4,5-dihydroimidazol-1-amine (log $P_{o/w}$ = 4.7)	100 ppm	3 % NaCl + static	72.1	[5]
1-(2-Aminoethyl)-2-heptadecyl imidazoline (log $P_{o/w}$ = 7.5)	0.1 g/L	1.65 % NaCl + Static @ 25 °C	99.4	[6]
2-(2-pyridyl)benzimidazole (log $P_{o/w}$ = 3.2)	7.68 mM	NACE brine ID196 + static @ 25 °C	67	[14]
2-(4-methoxyphenyl)- 4,5-diphenyl-imidazole (log $P_{o/w}$ = 5)	400 ppm	3.5 % NaCl + Static @ 25 °C	90	[15]
4,5-diphenyl-2-(p-tolyl)-imidazole (log $P_{o/w}$ = 5.4)	400 ppm	3.5 % NaCl + Static @ 25 °C	84	[15]
2-(4-nitrophenyl)-4,5- diphenyl-imidazole (log $P_{o/w}$ = 4.9)	400 ppm	3.5 % NaCl + Static @ 25 °C	77	[15]
Benzimidazole (log $P_{o/w}$ = –0.8)	100 ppm	5 % NaCl + Static @ 40 °C, pH 6	83	[16]
2-(2-pyridyl)benzimidazole (log $P_{o/w}$ = 3.2)	2.56 mM	Synthetic Brine +1000 rpm @ 25 °C	95	[17]
2-(2-Bromophenyl)-1-methyl-1H-benzimidazole (log $P_{o/w}$ = 3.8)	0.34 mM	3.5 % NaCl + Static @ 25 °C	97	[18]
1-(2-aminoethyl)-2(heptadec-8-enyl)-bis-imidazoline (log $P_{o/w}$ = 5.9)	100 ppm	3 % NaCl +1000 rpm @ 80 °C	98	[58]

reactivity of CMB; and accounts for the excellent inhibition performance obtained experimentally. This also accounts for the saturated distribution of total electron density of CMB as revealed in Fig. 12(b). The DFT data suggest strong disposition of CMB compound to interact with metal substrates which agrees with the experimental results. Going further, to evaluate the interaction/binding energy of CMB adsorption on Fe slab, molecular dynamic simulation was performed. The top and side views of the minimal energy adsorption orientations of CMB on Fe are presented in Fig. 13(a,b) respectively. The top view reveals flat-lying alignments with the N hetero-atoms of the 5-membered heterocyclic ring and C atoms of the benzene ring mostly accommodated within the vacant FCC groves: the so-called soft epitaxial adsorption orientation associated with minimal free energy of adsorption [56,57]. The MDS data in Table 7 reveal binding energy of -116.8 kcal/mol indicating enhanced adsorption strength thereby, agreeing with the experimental data.

3.5. Proposed mechanism of inhibition by CMB

At 25 °C in CO_2–saturated 3.5 % NaCl solution, the ability of CMB to shift E_{corr} value by more than 80 mV towards the anodic potential region provides the insight that CMB is a dominantly anodic–type sweet corrosion inhibitor. Consequently, CMB mitigates the sweet corrosion by blocking anodic transformation of Fe into Fe^{2+}. The inhibitor achieves this because it possesses free and reactive electrons domiciled around the C = C and N groups (based on DFT calculations), and because it is possible to exist as a protonated species in the acidic corrosion environment. The free electrons enable CMB to enter into a coordinate-covalent interaction with the Fe atoms through the filling of its empty d-orbitals. The protonated form enables CMB to interact electrostatically with adsorbed Cl^- ions on the steel surface. This interaction causes the formation of a protective CMB layer that cuts off the steel surface from

the corrosion agents. The formation of a CMB film is confirmed by the two time constants observed in the EIS results, the FTIR peaks detected on the inhibited steel surface, and the comparative composition of Fe on the steel surface based on EDAX analysis. However, the anodic inhibition mechanism of CMB is greatly influenced by the activity of Cl^- ions in the solution. By increasing the temperature of the CO_2–saturated 3.5 % NaCl solution up to 60 °C, the CMB adsorption on the steel surface weakens due to increased activity of the corrosion agents, especially, Cl^- species, as confirmed by the diminished low–frequency impedance peak in Fig. 9(b) and the EDAX results in Fig. 11(b & d). The antagonistic effect of Cl^- ions on the performance of CMB is further seen by the diminishing EIS peaks and their shift towards higher frequency as NaCl concentration reaches 7 %. Regardless, CMB has shown to be a highly effective sweet corrosion for C1018 carbon steel in CO_2–saturated NaCl solution. A comparison of performance between CMB and some sweet corrosion inhibitor reported in the literature is presented in Table 8.

4. Conclusion

In the oil industry, sweet corrosion is a major challenge [1]. The corrosion inhibition technology is adjudged the most cost-effective and flexible corrosion control measures [11–15]. In this work, 2–(chloromethyl)benzimidazole (CMB) has been explored as a potential corrosion inhibitor in CO_2–saturated NaCl solution under static condition. The influence of chloride ions concentration and temperature, which are common factors encountered in the sweet environment were also studied. Electrochemical studies with OCP, EIS and PDP indicate that CMB is highly effective in retarding the rate of charge transfer at the steel–solution interface. It achieves this by predominantly adsorbing on anodic sites and forming protective inhibitor layer on the steel surface, as ratified by FTIR characterization. The adsorption lowers the surface degradation of the carbon steel both at low and high temperatures up to 60 °C, according to SEM-EDAX characterizations. The adsorption is facilitated by the N–H, C = N, C = C moieties in CMB, based on FTIR and DFT results. The surface coverage of steel surface by CMB is enhanced by its flat adsorption orientation, based on quantum chemical calculations. However, the increase in temperature and NaCl concentration is detrimental to the integrity of the CMB–steel interface.

Acknowledgements

The authors acknowledge the support from the World Bank Africa Centers of Excellence for Impact (ACE Impact), Project No. NUC/ES/507/1/304. The Center of Research Excellence in Corrosion (CoRE–C), King Fahd University of Petroleum and Minerals, Saudi Arabia is also acknowledged for granting permission to use some of its equipment during this work.

5. *Declaration of interests*

The authors declare that they have no known competing financial interests or personal relationships that could have appeared to influence the work reported in this paper.

Declaration of Competing Interest

The authors report no declarations of interest.

References

[1] D.A. Lopez, T. Perez, S.N. Simison, The influence of microstructure and chemical composition of carbon and low alloy steels in CO_2 corrosion, A state-of-the-art appraisal, Mater. Des. 24 (2003) 561–575.
[2] H. Zhang, K. Gao, L. Yan, X. Pang, Inhibition of the corrosion of X70 and Q235 steel in CO_2–saturated brine by imidazoline–based inhibitor, J. Electroanal. Chem. 791 (2017) 83–94.
[3] H. Zhang, K. Gao, L. Yan, X. Pang, Inhibition of the corrosion of X70 and Q235 steel in CO_2–saturated brine by imidazoline–based inhibitor, J. Electroanal, Chem. 791 (2017) 83–94.
[4] D.A. Lopez, S.N. Simison, S.R. De Sanchez, Inhibitors performance in CO_2 corrosion: EIS studies on the interaction between their molecular structure and steel microstructure, Corros. Sci. 47 (2005) 735–755.
[5] P.C. Okafor, X. Liu, Y.G. Zheng, Corrosion inhibition of mild steel by ethylamino imidazoline derivative in CO_2-saturated solution, Corros. Sci. 51 (2009) 761–768.
[6] Y.Z. Li, N. Xu, X.P. Guo, G.A. Zhang, Inhibition effect of imidazoline inhibitor on the crevice corrosion of N80 carbon steel in the CO_2-saturated NaCl solution containing acetic acid, Corros. Sci. 126 (2017) 127–141.
[7] J. Zhao, F. Gu, D. Wang, M. Yu, Effects of thioureido imidazoline on the passivation and pitting corrosion of N80 steel in CO_2–saturated NaCl–$NaNO_2$ solution, Int. J. Electrochem. Sci. 13 (2018) 2676–2687.
[8] C.A. Gonzalez-Rodriguez, F.J. Rodriguez–Gomez, J. Genesca–Llongueras, The influence of Desulfovibrio vulgaris on the efficiency of imidazoline as a corrosion inhibitor on low-carbon steel in seawater, Electrochim. Acta 54 (1) (2008) 86.
[9] I. Jevremovic, M. Singer, S. Nesic, V. Miskovic-Stankovic, Inhibition properties of self-assembled corrosion inhibitor tall oil diethylenetriamine imidazoline for mild steel corrosion in chloride solution saturated with carbon dioxide, Corros. Sci. 77 (2013) 265–272.
[10] G. Zhang, C. Chen, M. Lu, C. Chai, Y. Wu, Evaluation of inhibition efficiency of an imidazoline derivative in CO_2-containing aqueous solution, Mater. Chem. Phys. 105 (2007) 331–340.
[11] V. Jovancicevic, S. Ramachandran, P. Prince, Inhibition of carbon dioxide corrosion of mild steel by imidazolines and their precursors, Corrosion 55 (1999) 449–455.
[12] https://pubchem.ncbi.nlm.nih.gov/compound/imidazoline.
[13] N-b-hydroxyethyl oleyl imidazoline, Material Safety Data Sheet, Sigma Aldrich, www.sigmaaldrich.com. (Retrieved 2 September, 2020).
[14] I.B. Onyeachu, I.B. Obot, A.A. Sorour, M.I. Abdul-Rashid, Green corrosion inhibitor for oilfield application I: electrochemical assessment of 2-(2-pyridyl) benzimidazole for API X60 steel under sweet environment in NACE brine ID196, Corros. Sci. 150 (2019) 183–193.
[15] A. Singh, K.R. Ansari, A. Kumar, W. Liu, C. Songsong, Electrochemical, surface and quantum chemical studies of novel imidazole derivatives as corrosion inhibitors for J55 steel in sweet corrosive environment, J. Alloys Compd. 712 (2017) 121–133.
[16] D.A. Lopez, T. Perez, S.N. Simison, The influence of microstructure and chemical composition of carbon and low alloy steels in CO2 corrosion, A state-of-the-art appraisal, Mater. Des. 24 (2003) 561–575.
[17] I.B. Onyeachu, I.B. Obot, A.Y. Adesina, Green corrosion inhibitor for oilfield application II: The time–evolution effect on the sweet corrosion of APIX 60 steel in synthetic brine and the inhibition performance of 2-(2-pyridyl)benzimidazole under turbulent hydrodynamics, Corros. Sci. 168 (2020), 108589.
[18] I.B. Obot, I.B. Onyeachu, S.A. Umoren, Alternative corrosion inhibitor formulation for carbon steel in CO_2-saturated brine solution under high turbulent flow condition for use in oil and gas transportation pipelines, Corros. Sci. 159 (2019), 108140.
[19] https://pubchem.ncbi.nlm.nih.gov/compound/2-4-Nitrophenyl-4,5-diphenyl-1H-imidazole.
[20] https://pubchem.ncbi.nlm.nih.gov/compound/2-_4-Methylphenyl_-4_5-diphenyl-1H-imidazole.
[21] https://pubchem.ncbi.nlm.nih.gov/compound/2-Phenylbenzimidazole.
[22] https://pubchem.ncbi.nlm.nih.gov/compound/2-_4-Bromophenyl_-1-methyl-1H-benzo_d_imidazole.
[23] https://pubchem.ncbi.nlm.nih.gov/compound/2-Chloromethylbenzimidazole.
[24] B. Yu-Bin, Z. An-Ling, T. Jiang-Jiang, G. Jin-Ming, Synthesis and Antifungal Activity of 2-Chloromethyl-1Hbenzimidazole derivatives against Phytopathogenic Fungi in Vitro, J. Agric, Food Chem. 61 (2013) 2759–2785.
[25] K. Petkar, P. Parekh, P. Mehta, A. Kumar, A. Baro, Synthesis & evaluation of 2-chloromethyl-1H-benzimidazole derivatives as antifungal agents, Int. J. Pharm. Pharm. Sci. 5 (2013) 115–119.
[26] E. Gutierrez, J.A. Rodriguez, J. Cruz-Borbolla, J.G. Alvarado–Rodriguez, P. Thangarasu, Development of a predictive model for the corrosion inhibition of carbon steel by imidazole and benzimidazole derivatives, Corr. Sci. 108 (2016) 23–35.
[27] K.F. Khaled, Experimental and computational investigations of corrosion and corrosion inhibition of iron in acid solutions, J. Appl, Electrochem. 41 (2011) 277–287.
[28] A.P. Srikanth, T.G. Sunitha, V. Raman, S. Nanjundan, N. Rajendran, Synthesis, characterization and corrosion protection properties of poly (n-(acryloyloxymethyl) benzotriazole-co-glycidyl methacrylate) coatings on mild steel, Mater. Chem. Phys. 103 (2007) 241–247.
[29] E.E. Oguzie, Y. Li, F.H. Wang, Corrosion inhibition and adsorption behavior of methionine on mild steel in sulphuric acid and synergistic effect of iodide ion, J. Colloid Interface Sci. 310 (2007) 90–98.
[30] J.F. Harvey, D.P. Schweinsberg, A guide to polarization curve interpretation: Deconstruction of experimental curves typical of the Fe/H_2O/H+/O_2 corrosion system, Corros. Sci. 47 (2005) 2125–2156.
[31] C.C. Ahanotu, I.B. Onyeachu, M.M. Solomon, I.S. Chikwe, O.B. Chikwe, C. A. Eziukwu, *Pterocarpus santalinoides* leaves extract as a sustainable and potent inhibitor for low low carbon steel in a simulated pickling medium, Sustain. Chem. Pharm. 15 (2020).
[32] Q.B. Zhang, Y.X. Hua, Corrosion inhibition of mild steel by alkylimidazolium ionic liquids in hydrochloric acid, Electrochim. Acta 54 (2009) 1881–1887.

[33] I.B. Onyeachu, D.S. Chauhan, K.R. Ansari, I.B. Obot, M.A. Quraishi, A.H. Alamri, 6-bis(N-D-glucopyranosylamine) as a novel corrosion inhibitor for oil and gas industry: electrochemical and computational analysis, Hexamethylene-1, New. J. Chem. (2019) 7282–7293.
[34] R. Fuchs-Godec, M.G. Pavlovic, Synergistic effect between non-ionic surfactant and halide ions in the forms of inorganic or organic salts for the corrosion inhibition of stainless-steel X4Cr13 in sulphuric acid, Corros. Sci 58 (2012) 192–201.
[35] M.M. Solomon, H. Gerengi, T. Kaya, E. Kaya, S.A. Umoren, Synergistic inhibition of St37 steel corrosion in 15% H_2SO_4 solution by chitosan and iodide ion additives, Cellulose 24 (2017) 931–950.
[36] R. De Levie, The influence of surface roughness of solid electrodes on electrochemical measurements, Electrochim. Acta 10 (2) (1965) 113–130.
[37] W. Zhang, H.J. Li, Y. Wang, Y. Liu, Q.Z. Gu, Y.C. Wu, Gravimetric, electrochemical and surface studies on the anticorrosive properties of 1-(2-pyridyl)-2-thiourea and 2-(imidazol-2-yl)-pyridine for mild steel in hydrochloric acid, New J. Chem. 42 (15) (2018) 12649–12665.
[38] S. Nesic, J. Postlethwaite, S. Olsen, An electrochemical model for prediction of corrosion of mild steel in aqueous carbon dioxide solutions, Corrosion 52 (1996) 280–294.
[39] H. Fang, B. Brown, S. Nesic, Sodium chloride concentration effects on general CO_2 corrosion mechanisms, Corros. 69 (2013) 297–302.
[40] Z. Zeng, R.S. Lilard, H. Cong, Effect of salt concentration on the corrosion behavior of carbon steel in CO_2 environment, Corros. 72 (6) (2016) 805–823.
[41] J. Han, J.W. Carey, J. Zhang, Effect of sodium chloride on corrosion of mild steel in CO_2-saturated brines, J. Appl, Electrochem. 41 (2011) 741–749.
[42] J. Han, J.W. Carey, J. Zhang, Effect of sodium chloride on corrosion of mild steel in CO_2-saturated brines, J. Appl, Electrochem. 41 (2011) 741–749.
[43] M.B. Kermani, L.M. Smith, Predicting CO_2 corrosion in the oil and gas industry, In: EUROCORR Annual Congress, 30 October-3 November, Bournemouth, U.K. (1994).
[44] I.B. Obot, I.B. Onyeachu, S.A. Umoren, M.A. Quraishi, A.A. Sorour, T. Chen, N. Aljeaban, Q. Wang, High temperature sweet corrosion and inhibition in the oil and gas industry: Progress, challenges and future perspectives, J. Pet, Sci. Eng. 185 (2020), 106469.
[45] G. Lin, M. Zheng, Z. Bai, X. Zhao, Effect of temperature and pressure on the morphology of carbon dioxide corrosion scales, Corros. 62 (2006) 501–507.
[46] N.T. Abdel Ghani, A.M. Mansour, Molecular structure of 2-chloromethyl-1H-benzimidazole hydrochloride: Single crystal, spectral, biological studies, and DFT calculations, Spectrochimica Acta Part A 86 (2012) 605–613.
[47] N. Sundaraganesan, S. Ilakiamani, P. Subramani, B.D. Joshua, Comparison of experimental and ab initio HF and DFT vibrational spectra of benzimidazole, Spectrochimica Acta Part A 67 (3-4) (2007) 628–635.
[48] S.K. Saha, P. Ghosh, A. Hens, N.C. Murmu, P. Banerjee, Density functional theory and molecular dynamics simulation study on corrosion inhibition performance of mild steel by mercapto-quinoline Schiff base corrosion inhibitor, Phys. E Low-Dimens. Syst. Nanostructures. 66 (2015) 332–341, https://doi.org/10.1016/j.physe.2014.10.035.
[49] M. Yadav, R.R. Sinha, T.K. Sarkar, N. Tiwari, Corrosion inhibition effect of pyrazole derivatives on mild steel in hydrochloric acid solution, J. Adhes, Sci. Technol. 29 (2015) 1690–1713.
[50] M. Yadav, R.R. Sinha, T.K. Sarkar, N. Tiwari, Corrosion inhibition effect of pyrazole derivatives on mild steel in hydrochloric acid solution, J. Adhes, Sci. Technol. 29 (2015) 1690–1713.
[51] M.A. Chidiebere, C.E. Ogukwe, K.L. Oguzie, C.N. Eneh, E.E. Oguzie, Corrosion Inhibition and Adsorption Behavior of Punicagranatum Extract on Mild Steel in Acidic Environments : Experimental and Theoretical Studies (2012) 668–677.
[52] D.I. Njoku, Y. Li, H. Lgaz, E.E. Oguzie, Dispersive adsorption of *Xylopia aethiopica* constituents on carbon steel in acid-chloride medium: A combined experimental and theoretical approach, J. Mol, Liq. 249 (2018).
[53] L.C. Murulana, M.M. Kabanda, E.E. Ebenso, Experimental and theoretical studies on the corrosion inhibition of mild steel by some sulphonamides in aqueous HCl, RSC Adv. 5 (2015) 28743–28761, https://doi.org/10.1039/c4ra11414k.
[54] B. Xu, W. Yang, Y. Liu, X. Yin, W. Gong, Y. Chen, Experimental and theoretical evaluation of two pyridine carboxaldehyde thiosemicarbazone compounds as corrosion inhibitors for mild steel in hydrochloric acid solution, Corros. Sci. 78 (2014) 260–268, https://doi.org/10.1016/j.corsci.2013.10.007.
[55] S.K. Saha, A. Dutta, P. Ghosh, D. Sukul, P. Banerjee, Adsorption and corrosion inhibition effect of Schiff base molecules on the mild steel surface in 1 M HCl medium: a combined experimental and theoretical approach, Phys. Chem. Chem. Phys. 17 (2015) 5679–5690, https://doi.org/10.1039/C4CP05614K.
[56] D.I. Njoku, E.E. Oguzie, Y. Li, Characterization, electrochemical and theoretical study of the anticorrosion properties of *Moringa oleifera* extract, J. Mol, Liq. 237 (2017) 247–256.
[57] E.E. Oguzie, Y. Li, S.G. Wang, F. Wang, Understanding corrosion inhibition mechanisms—experimental and theoretical approach, RSC Adv. 1 (2011), https://doi.org/10.1039/c1ra00148e.
[58] F. Farelas, A. Ramirez, Carbon dioxide corrosion inhibition of carbon steels through bis-imidazoline and imidazoline compounds studied by EIS, Int. J. Electrochem. Sci. 5 (1) (2010) 797–814.